# A dual-basis pursuit reconstruction technique for tomographic PIV

**Conference Paper** · July 2014

CITATION
1

READS
188

**4 authors**, including:

Qi Gao
Zhejiang University
**62** PUBLICATIONS **670** CITATIONS
SEE PROFILE

Hong Ping Wang
Chinese Academy of Sciences
**38** PUBLICATIONS **340** CITATIONS
SEE PROFILE

Jinjun Wang
Beihang University (BUAA)
**245** PUBLICATIONS **3,867** CITATIONS
SEE PROFILE

# A dual-basis pursuit reconstruction technique for tomographic PIV

**ZhiJian Ye[1], Qi Gao[1,*], HongPing Wang[1], JinJun Wang[1]**

1: Institute of Fluid Mechanics, Beijing University of Aeronautics and Astronautics, Beijing, China
* correspondent author: qigao@buaa.edu.cn

**Abstract** As an inverse problem, particle reconstruction in tomographic particle image velocimetry (Tomo-PIV) attempts to solve a large-scale underdetermined linear system using optimization technique. The most popular approach, multiplicative algebraic reconstruction technique (MART), uses entropy as objective function in the optimization. All studies on MART-based techniques are focusing on improving efficiency and accuracy of particle reconstruction in Tomo-PIV. However, they do not perform very well on dealing with ghost particles in a very dense particle field. A new technique for tomographic particle reconstruction is proposed based on basis pursuit technique. A template basis is introduced as an *a priori* knowledge of particle intensity distribution combined with a correcting basis to span the solution space of the underdetermined linear system. A numerical assessment test with 2D synthetic images indicates that the new dual-basis pursuit (DBP) technique is superior to MART method, which can completely recover the particle field with $ppp < 0.15$, and keep the quality factor $Q$ above 0.8 for particle per pixel (ppp) up to 0.30. Furthermore, dual-basis MART (DB-MART) and dual-basis SMART (DB-SMART) are tested in 2D numerical assessment test, which both have better performance than original MART and SMART. Due to the difficulty of applying DBP to 3D application regarding unaffordable memory usage and time consuming, only DB-MART and DB-SMART are doable for 3D particle reconstruction in a large domain. Therefore, a 3D synthetic experiment is performed to assess the DB-SMART method.

## 1. Introduction

Due to the outstanding performance on doing a three-dimensional three-component (3D3C) velocity measurement, tomographic particle image velocimetry (Tomo-PIV) has rapidly become a versatile and accurate approach of volumetric measurement (Elsinga, Scarano et al. 2006; Scarano 2013). The technique mainly relies on the reconstruction of the three-dimensional distribution of tracer particles. It obtains the three-dimensional particle distribution by analyzing images of particles (3 or 4 in general) that are simultaneously recorded from different viewing angles. The three-component velocity field in the measure volume is then achieved by volumetric cross-correlation.

The iterative algebraic methods (Herman and Lent 1976) are commonly used to tomographic reconstruction since they are simple, versatile and have the ability to handle under-sampled and large-scale data even with noise (Natterer 1999). Multiplicative algebraic reconstruction technique (MART) was firstly introduced into volumetric PIV by Elsinga et al. (Elsinga, Scarano et al. 2006), which was originally proposed by Gordon et al. (Gordon, Bender et al. 1970) for medical tomography. In mathematic term, MART tries to solve underdetermined equation system under the theory of maximum entropy. The technique broadens the thoughts and promotes the development of volumetric velocity measurements. Atkinson and Soriano (Atkinson and Soria 2009) developed a simultaneous multiplicative algebraic reconstruction technique (SMART), which made a significant improvement on computing time and memory usage of the algorithm without losing accuracy. Numerous MART-based approaches were developed to improve the efficiency and accuracy of 3D particle reconstruction. However, issues of ghost particle and seeding density are obstacles to achieve a better spatial resolution on measurements using MART-based techniques.

Recently, people have realized that a few important features of particle distribution did not benefit the tomographic reconstruction, which are sparsity and spherical intensity distribution of particle (Petra, Schnörr et al. 2007). Sparsity, in other word, means that most voxels (more than 95%) of particle intensities are zero (Westerweel, Elsinga et al. 2013). Only the area that occupied by tracer particles have non-zero intensity. Obviously, many researchers have known this characteristic and used it to optimize the technique for both MART and SMART. Multiplicative first guess (MFG) proposed by Worth and Nickels (Worth and Nickels 2008) and multiplicative line of sight (MLOS) by Aktinsom and Soria (Atkinson and Soria 2009) both use

this characteristic to provide an optimized initial intensity distribution of particle for iteration. Both methods accelerate the convergence of result and reduce the computational cost. Recent development of compressed sensing (Donoho 2006) provides an effective tool for the process of sparse and under-sampled signal, which has been noticed probably practicable for tomographic reconstruction. Petra *et al.* (Petra, Schröder et al. 2009; Petra and Schnörr 2010) have done systematic investigations in this field, which mainly focus on two questions: (a) under what seeding density, the 3-dimensional particle distribution will be reconstructed accurately (without ghost particles); (b) Under what conditions, the $l_0$-norm can be replaced by $l_1$-norm as an objective function in optimization solver? The entire mathematics frame has been established, while it is about to apply the approach to real experimental measurements.

Spherical intensity distribution of a particle regards an *a priori* knowledge that the basic shape of the object to be reconstructed in Tomo-PIV is a small particle with uniform size. This feature associates with the physical model of weight function of particle projection suggested in MART and SMART, namely cylinder-sphere intersection (Lamarche and Leroy 1990). It results in reconstructing a particle with almost same diameter as image particles, which forming a few pixels blob due to the diffraction of tracer particle. The *a priori* knowledge was also discussed by Petra et al (Petra, Schnörr et al. 2007), where they proposed Gaussian-type basis function to simulate the particle intensity distribution. It grabs more attentions in this field recently. Multiple ways of implementing the spherical intensity distribution into tomographic reconstruction were proposed, such as optical transfer function (Schanz, Gesemann et al. 2013), point spread function (Champagnat, Cornic et al. 2013) and spatial filter (Discetti, Natale et al. 2013).

Therefore, taking features of the sparsity and spherical intensity distribution of particle into account for Tomo-PIV reconstruction is new trend to improve the particle reconstruction algorithm. We propose a dual-basis pursuit (DBP) technique, and combine it with MART and SMART to improve current particle reconstruction methods. In Sect. 2, a brief introduction of the mathematical problem behind tomographic reconstruction is provided, and the concept of dual-basis is defined in details. 2D tests of the new technique are investigated in Sect. 3, while an application of 3D synthetic flow is performed in Sec. 4.

## 2. Dual-basis technique

### *2.1 The reconstruction problem*

The physical problem of the particle reconstruction in Tomo-PIV is: how can we deduce an unknown 3D particle distribution, if projections of this particle field on multiple cameras are known? In a mathematical word, the issue is about solving an inverse problem. If the unknown 3D particle distribution is described as a 3D intensity matrix $\mathbf{E}$ with size of $n_x \times n_y \times n_z$, it can be reshaped to a column matrix of $\mathbf{E}_{n\times 1}$ with $n = n_x \times n_y \times n_z$. Here, same matrix symbol with and without '~' represent 3D matrix and its reshaped column matrix, respectively, unless the dimensions of a matrix are emphasized with subscripts. The projection function can be discretized as a transformation matrix $\mathbf{W}_{m\times n}$ (weighting matrix), which projects the $\mathbf{E}$ to its 2D intensity $\mathbf{I}_{m\times 1}$ on camera. Here, $m$ is the number of all pixels that record the projection of $\mathbf{E}$. The weighting matrix $\mathbf{W}_{m\times n}$ was calculated using cylinder-sphere intersection model (Lamarche and Leroy 1990) in current work. Therefore, the mathematics behind particle reconstruction is solving a linear equation system:

$$\mathbf{WE} = \mathbf{I}, E_s \geq 0, (1 \leq s \leq n), \tag{1}$$

where $s$ is the 1D index associate with 3D indexes of $\mathbf{E}$, at location of ($i_s$, $j_s$, $k_s$).

Unfortunately, Eq. 1 is a large-scale underdetermined linear system, since $n$ is much larger than $m$. To make the problem solvable, one way is to transform the problem to be an optimization problem. Consequently, an objective function $f(\mathbf{E})$ is required, and the problem becomes:

$$\min f(\mathbf{E}) \text{ or } \max f(\mathbf{E}); \text{s.t.} \begin{cases} \mathbf{WE} = \mathbf{I}, \\ E_s \geq 0, (1 \leq s \leq n). \end{cases} \tag{2}$$

For the basic reconstruction technique of Tomo-PIV, multiplicative algebraic reconstruction technique (MART), the concept of the objective function is information entropy, namely

$$f(\mathbf{E}) = -\sum_{s=1}^{n}(E_s / E^*)\ln(E_s / E^*), E^* = \sum_{s=1}^{n} E_s, \tag{3}$$

while its prototype, algebraic reconstruction techniques (ART), defines the objective function as $l_2$-norm of $\mathbf{E}$ (Gordon, Bender et al. 1970). All available MART-based techniques used for Tomo-PIV reconstruction are based on entropy criterion. More details of MART-based algorithms are currently well reviewed by Scarano (Scarano 2013) and Gao et al. (Gao, Wang et al. 2013).

On the other hand, Eq. 2 has four behaviors (**B1-B4**) of the constraints (Petra, Schnörr et al. 2007; Barbu, Herzet et al. 2011):

**B1:** The linear equations are very large-scale underdetermined systems;

**B2:** $\mathbf{E}$ is a sparse column matrix;

**B3:** $\mathbf{E}$, in its 3D format ($\mathbf{E}$), has a local pattern of solution, which is the basic intensity distribution of a particle;

**B4:** Elements of $\mathbf{E}$ are all non-negative, $E_s \geq 0$.

To solve this kind of underdetermined linear system with sparse solution, a classical NP-hard problem, mathematicians developed various tools, e.g. matching pursuit (Mallat and Zhang 1993), basis pursuit (Chen, Donoho et al. 1998) and compressed sensing (Donoho 2006). These technique have been well accepted and spread their applications to various fields including fluid mechanics.

The new technique (compressed sensing) normally utilizes $l_q$-norm ($0 \leq q \leq 1$) as objective function, which has strong physical meaning in image processing under condition of $E_s \geq 0$. $l_1$-norm represents the summation of $\mathbf{E}$, which have been studied in Gesemann et al. (Gesemann, Schanz et al. 2010), named as L1-regularized, while $l_0$-norm indicates the total number of positive elements of $\mathbf{E}$. In L1-regularized method, Eq. (2) is solved under the objective function $l_1$-norm of $\mathbf{E}$. Petra and Schröder (Petra, Schröder et al. 2009) built up a theoretical framework of application of compressed sensing on Tomo-PIV reconstruction. However, the basic concept of compressed sensing does not take the benefit of behavior **B3**, which is a potential *a priori* constraint. Petra et al. (Petra, Schnörr et al. 2007) pointed out that current reconstruction techniques (ART-based or MART-based methods) have limitation due to the lack of applying **B3**. To make the **B3** involved for particle reconstruction, manual intervention is needed to restrict/guide the iteration. Using a template of particle intensity distribution for solving $\mathbf{E}$ is an ingenious idea, such as using Gaussian-type basis function (Petra, Schnörr et al. 2007) or point spread function (Champagnat, Cornic et al. 2013; Cornic, Champagnat et al. 2013), and then the optimization problem becomes:

$$\min f(\mathbf{E}^{'}); s.t. \begin{cases} \mathbf{WME}^{'} = \mathbf{I}, \\ E_s^{'} \geq 0, (1 \leq s \leq n), \end{cases} \tag{4}$$

where $\mathbf{M}_{n\times n}$ is the basis function regarding particle template, $\mathbf{E}_{n\times 1}^{'}$ is the projection coefficient satisfying

$$\mathbf{E} = \mathbf{ME}^{'} \tag{5}$$

In a template-based optimization method, the basis function can not only restrict the solution to having a good locally isotropic intensity distribution, but also accelerate the iteration of reaching a sparse solution. Cornic el al. (Cornic, Champagnat et al. 2013) first investigated the performance of the compressive sampling matching pursuit (CoSaMP) on tomographic reconstruction. Combining with a local maxima detection algorithm, the CoSaMP approach clearly outperforms classical SMART. However, designing an appropriate set of basis is not an easy task. Theoretically, a set of linearly independent bases can span a convex space $R^n$ without constraint **B4**. When $\mathbf{E}, \mathbf{M}, \mathbf{E}^{'}$ are all positive, the bases have to be orthogonal bases. Therefore, the goal of this work is finding a n-rank particle-template-based matrix $\mathbf{M}$ to span a convex solution space $R^n$ ($\mathbf{E} \in \mathbf{R}^n$) with non-negative projection coefficient $\mathbf{E}^{'}$.

### *2.2 Dual-basis pursuit*

Eq. 5 well describes the idea of basis pursuit technique that a discrete signal $\mathbf{E}$ can be decomposed as a linear combination, or an approximation as:

$$\mathbf{E} = \mathbf{M_1 E_1^{'}} + \boldsymbol{\varepsilon}, \tag{6}$$

where $\mathbf{M_1}$ and $\mathbf{E_1^{'}}$ are basis matrix and coefficient column matrix like $\mathbf{M}$ and $\mathbf{E}^{'}$, respectively. $\boldsymbol{\varepsilon}_{n\times 1}$ is a residual. In tomographic PIV reconstruction, blob-like template bases are superior candidates for $\mathbf{M}_1$, but not easy to make them orthogonal, which means they can only span a sub-space of the solution space if $\mathbf{E_1^{'}} \geq 0$. In other words, a set of linearly independent template basis could not reconstruct a 3D particle field with sub-voxel accuracy. Consequently, there is a residual $\boldsymbol{\varepsilon}$ in Eq. (6). However, $\boldsymbol{\varepsilon}$ can also be decomposed into a linear combination of a standard basis $\mathbf{M}_2$ with coefficient $\mathbf{E}_2^{'} \geq 0$, resulting in:

$$\mathbf{E} = \mathbf{M}_1\mathbf{E}_1^{'} + \mathbf{M}_2\mathbf{E}_2^{'} \tag{7}$$

We name $\mathbf{M}_1$ as template basis (TB) and $\mathbf{M}_2$ as correcting basis (CB). In this work, a Gaussian basis function is used for TB. To describe the TB, $\mathbf{M}_1^{(s)}$ is defined as the 3D format of $\mathbf{M}_1^s$, the $s$-th column matrix of $\mathbf{M}_1$. Thus,

$$\mathbf{M}_{1,ijk}^{(s)} = \begin{cases} C_1 \exp(-\dfrac{\| \mathbf{p}-\mathbf{p}_s \|_2^2}{2\sigma^2}), \text{if } \| \mathbf{p}-\mathbf{p}_s \|_2 \leq D/2, \\ 0, \text{if } \| \mathbf{p}-\mathbf{p}_s \|_2 > \mathrm{D}/2. \end{cases} \tag{8}$$

Where constant $C_1$ is the maximum intensity of Gaussian basis, $\sigma$ is the standard deviation of Gaussian distribution, $p=(i,j,k)$, $p_s=(i_s,j_s,k_s)$, and $D$ is the diameter of the particle template. Practically, parameters of $C_1$ and $\sigma$ are obtained from an averaged 2D particle intensity distribution from projections of individual particles on cameras. $D$ can be set to $4\sigma$ for guaranteeing including 95% intensity. Similarly, the $s$-th column matrix of $\mathbf{M}_2$ is defined as:

$$\mathbf{M}_{2,ijk}^{(s)} = \begin{cases} C_2, \text{if } \mathbf{p} = \mathbf{p}_s \\ 0, \text{if } \mathbf{p} \neq \mathbf{p}_s. \end{cases} \tag{9}$$

Where $C_2$ is a constant intensity of CB, which could normally be set as $C_2 = C_1$. Therefore, $\mathbf{M}_2$ is proportional to identity matrix. Fig. 1 explain the roles of TB and CB on reconstructing a particle (a 1D example). TB is a symmetric model of intensity distribution, while CB can help to shift the peak of intensity to have a sub-grid accuracy. Therefore, any particle intensity distribution is equal to a combination of TB and CB as Eq. 7. In DBP, $l_1$-norm of $\mathbf{E}_2^{'}$ is defined as the objective function. Minimizing $\| \mathbf{E}_2^{'} \|_1$ means maximizing the correlation between the real intensity distribution and the template basis, which makes the objective function bounded. Therefore, the optimization problem becomes

$$\min \| \mathbf{E}_2^{'} \|_1 ; s.t. \begin{cases} \mathbf{W}(\mathbf{M}_1\mathbf{E}_1^{'} + \mathbf{M}_2\mathbf{E}_2^{'}) = \mathbf{I} \\ E_{1,s}^{'}, E_{2,s}^{'} \geq 0, (1 \leq s \leq n) \end{cases} \tag{10}$$

Since both constraints and the objective function are linear, Eq.10 can be solved using a linear program algorithm.

According to the following 2D test, we have known that DBP can produce better result (see Fig. 2) but it is not easy to extend it to 3D applications due to the unaffordable computer memory and time cost. For making good use the concept of dual-basis, we propose other methods by combining the dual-basis method and the MART/SMART algorithms

### *2.3 Dual-basis MART and SMART*

As is mentioned above, MART and SMART can be used to solve the optimization problem of Eq.2. Now we use MART and SMART to solve Eq.4. Here, we transform the Eq.4 to general case:

$$\min f(\mathbf{E}^{'}); s.t. \begin{cases} \mathbf{B}\mathbf{E}^{'} = \mathbf{I}, \\ \mathbf{E}_s^{'} \geq 0, (1 \leq s \leq n), \end{cases} \tag{11}$$

where, $\mathbf{B} = \mathbf{W}\mathbf{M}$. Now, the Eq.11 is similar to the Eq.2, and then the same iteration of MART and SMART can be used to solve this problem. We name them DB-MART and DB-SMART, respectively. Namely:

**DB-MART:**

$$E'(X_j,Y_j,Z_j)^{k+1} = E'(X_j,Y_j,Z_j)^k (I(x_i,y_i) / \sum_{j\in N_i} b_{ij} E'(X_j,Y_j,Z_j)^k)^{\mu b_{ij}} \quad (12)$$

where $(X_j,Y_j,Z_j)$ is the coordinate of $j$-th voxel; $(x_i,y_i)$ is the coordinate of $i$-th pixel; $b_{ij}$ is the element of $\mathbf{B}$; $\mu$ is a scalar relaxation parameter.

**DB-SMART:**

$$E'(X_j,Y_j,Z_j)^{k+1} = E'(X_j,Y_j,Z_j)^k \prod_i^{N_i} [(I(x_i,y_i) / \sum_{j\in N_i} b_{ij} E'(X_j,Y_j,Z_j)^k)^{\mu b_{ij}}]^{1/N_i} \quad (13)$$

The initial value of DB-MART and DB-SMART can be estimated using MFG and MLOS as well.

**MFG:**

$$E_0' = \left[ \prod_{k=1}^{N_c} \left( \sum_{i=N_k^o}^{i=N_k^{end}} b_{ij} I_i \right) \right]^{1/N_c} \quad (14)$$

where $N_c$ is the number of cameras, $N_k^o$ and $N_k^{end}$ is the first and last index of the $k$-th camera.

**MLOS:**

$$E_0' = \left[ \prod_{i=1}^{m} \left( I_i^{b_{ij}} \right) \right]^{1/N_c} \quad (15)$$

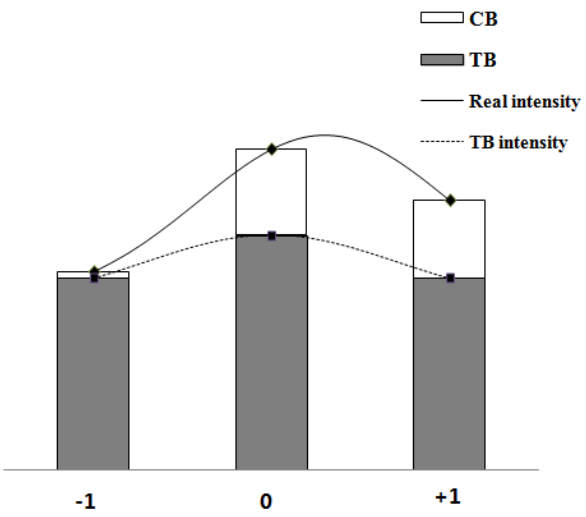


**Fig.** 1 Schematic of TB and CB (one-dimensional). A combination of TB and CB achieve a sub-grid intensity distribution.

## 3. Numerical assessment

The performances of DBP, DB-MART and DB-SMART were assessed via a typical 2D numerical test of tomographic PIV reconstruction for algorithm study, same as the 2D test by Elsinga et al. (Elsinga, Scarano et al. 2006) and Discetti el al. (Discetti, Natale et al. 2013). Unless stated otherwise, synthetic particles with size of $3\times 3$ voxels were randomly generated and distributed in a 2D test domain of $1000\times 200$ grids. Synthetic particles had Gaussian intensity distribution with a maximum intensity of 200 counts and standard deviation of $\sigma_s$=0.75 pixels, which was 1/4 of the particle size (Adrian and Westerweel 2010). Projections of particles on four virtual cameras (1D projection) were synthesized. Four cameras were aligning with equal difference of viewing angle of $20^\circ$, resulting in a total viewing range of $60^\circ$. The TB was defined as Eq.8 with $C_1$ = 1, $\sigma = \sigma_s$ =0.75 , and $D$ =4$\sigma$ . $C_2$ was set to equal to $C_1$ for CB.

Different algorithms were tested for comparison. All settings of the tested methods are summarized as:

the MART used standard settings of 5 iteration steps and relaxation factor = 1; The SMART set the relaxation factor to 1 and the iteration steps to 80; The DB-MART and DB-SMART had the same settings as MART and SMART, respectively; The DBP and L1-regularized were solved using linear programming method. The exit condition of the iteration was the residual between the origin projections and new projections of the reconstructed volume below a certain critical value, which was 0.1. Both DBP and L1-regularized were implemented in the environment of MATLAB using the optimization function *linprog* with algorithm of 'large-scale interior-point'.

Fig. 2 shows the test results of the normalized correlation coefficient $Q$ (Elsinga, Scarano et al. 2006) of the exact and reconstructed intensity distribution under various seeding densities. A significant improvement of particle reconstruction was achieved by using dual-basis pursuit technique. For particle field of ppp less than 0.15, the DBP technique can completely recover the particle distribution with $Q >$ 0.99, while for ppp larger than 0.3, it makes the correlation coefficient $Q$ stay above 0.8, when the particle field is too dense to be reconstructed well using all other algorithms. For L1-regularized method, it only shows good performance at small seeding density (ppp < 0.1), and rapidly becomes worse with increase of seeding density. It becomes even worse than DB-MART and DB-SMART algorithms when tracer concentration above 0.2ppp. The difference between DBP and L1-regularized indicates the importance of template basis, which is also verified by the performance of DB-MART and DB-SMART versus MART and SMART. After adding the template basis, both DB-MART and DB-SMART have better performance than MART and SMART. The improvement between DBP and DB-MART/DB-SMART suggests that the feature of sparsity as discussed in Sec. 1 (different objective functions) is another valuable behavior that can be used to advance current particle reconstruction approaches.

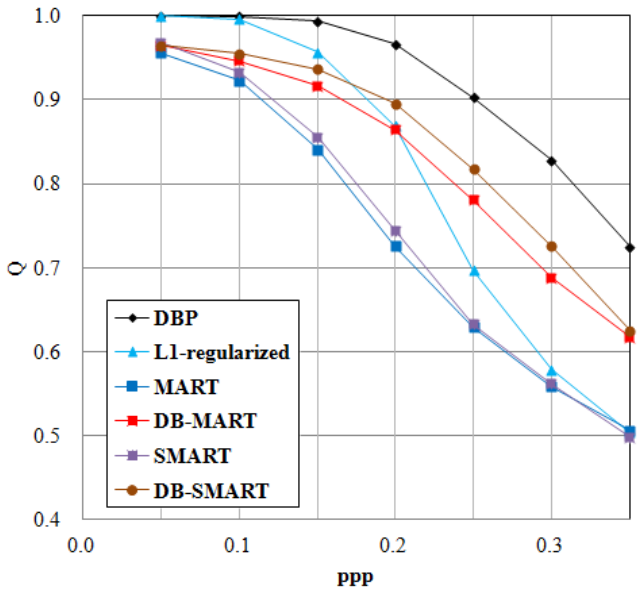


**Fig. 2** Comparison of different reconstruction techniques in terms of quality factor $Q$ with varying seeding density of unit ppp.

Due to the difficulty of applying DBP to 3D application regarding memory usage and time consuming, only DB-MART and DB-SMART are doable for 3D particle reconstruction in a large domain. Therefore, only DB-SMART is focused in following sections.

### *3.1 Effect of the standard deviation of template basis in DB-SMART*

The tracer particles are very small in general. Their projections on image are mainly the Airy spots due to diffraction, which can be approximated as Gaussian intensity distribution (Adrian and Westerweel 2010). Normally, the size and shape of particle images can be considered uniform, which means the standard deviation and diameter of particle images are uniform. On the other hand, the reconstructed 3D particles are assumed to have the same standard deviation as well as the particle images. In tomo-PIV measurement, the standard deviation and size of particle image are statistically obtained for generating TB in DB-SMART.

When uncertainties exist on the standard deviation for TB, it definitely affects the accuracy of the algorithm. Therefore, parametric study on robustness of the standard deviation were conducted. Fig. 3 shows the effect of standard deviation on the quality factor. The standard deviation of synthetic particles varies from 0.5 to 1.5 (the diameter of synthetic particles varies from 2 to 6), while the standard deviation of TB remains 0.75. It suggests that the less difference between the standard deviations of particle image and TB causes the smaller reducing of *Q*. Within the range of $\sigma = 0.5 \sim 1$ (~30% difference), decrease of *Q* is under 5% that is acceptable. *Q* drops rapidly when the difference is beyond 30% ($\sigma > 1$).

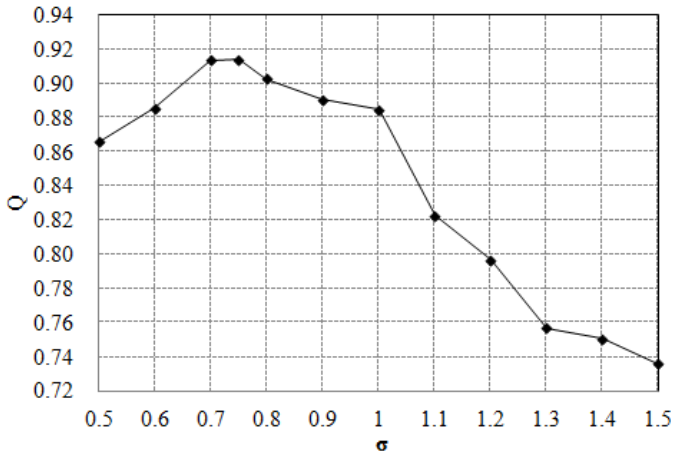


**Fig. 3** The effect of standard deviation. The standard deviation of synthetic particles vary from 0.5 to 1.5 while the template basis remains 0.75. Here, $ppp$ = 0.15, $\mu$ =1 and the steps of iteration is 80.

### *3.2 Effect of the noise in DB-SMART*

In this section, two type of noise are studied: random noise added to the images and background particles located outside the reconstruction volume (Elsinga, Scarano et al. 2006). Fig. 4 shows the effect of random noise (white noise). The noise level is the percentage of the particle peak intensity. Fig. 5 shows the effect of background particles. Both types of noise cause decreasing of *Q* linearly. Between these two types of noise, it seems that random noise on images has larger influence on the reconstruction. *Q* reduces about 20% when random noise goes up to 50%. When background particles rises to 50%, it means about 1/3 particle images are unmatched among cameras, which is fairly a high disturbance on particle reconstruction. However, it only causes about 10% worse of *Q*.

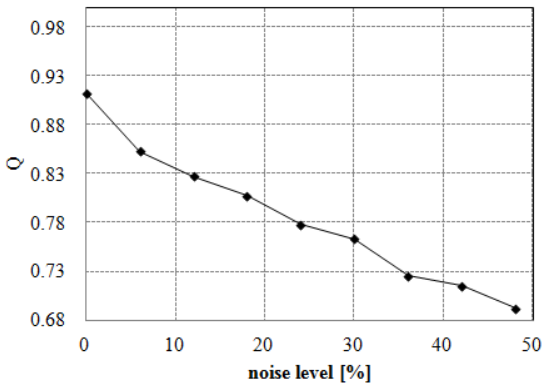


**Fig. 4** Effect of random noise on the reconstruction

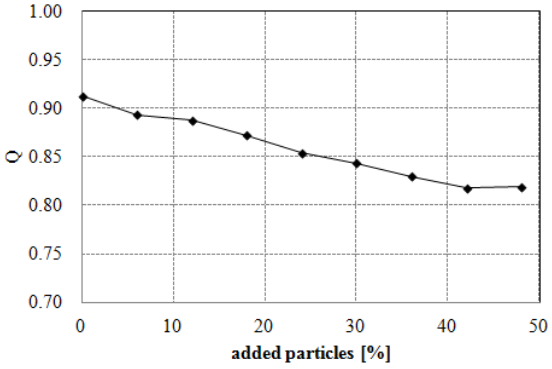


**Fig. 5** Effect of background particles on the reconstruction

## 4. Synthetic 3D experiment

For 3D application, a synthetic 3D experiment was performed by a simulation of particle motion field around a ring vortex, which is classical test case designed by Elsinga et al. (Elsinga, Scarano et al. 2006). The measure volume was $35\times35\times7$ mm$^3$ ($700\times700\times140$ voxels). 24500 tracer particles were generated and randomly distributed in the field to achieve a seeding density of 0.05ppp. The diameter and standard deviation of synthetic particles are 3 voxels and 0.75 voxels with maximal intensity 200 counts. Each of four square-arranged cameras has a $30^{\circ}$ viewing angle (to the left, right, upward and downward).

DB-SMART was used to reconstruct the 3D intensity distribution with 80 iterations and $\mu$ = 1, which returned a particle field of $Q$ =0.90. The displacement field was obtained via correlation of volume deformation iterative multigrid (VODIM) (Scarano and Poelma 2009) using $32^3$ interrogation volume with 75% overlap. Therefore, the measured displacement field contains $84\times84\times14$ vectors shown in Fig. 6. The iso-surface corresponding to a vorticity magnitude of 0.13voxels/voxel returns the expected vortex ring. Five planes of velocity vectors are also displayed. The color-coding indicates the magnitude of the velocity vector.

The measurement accuracy is presented in the form of 2D scatter plots of the displacement error (Fig. 7), where 90% of the vectors have an absolute error smaller than 0.07 and 0.07 voxels in x and y directions, and less than 0.12 voxels in z. The root-mean-square of $\Delta u$ ($x$ displacement error) and $\Delta v$ are 0.050 and 0.05 respectively, while 0.08 in z-direction.

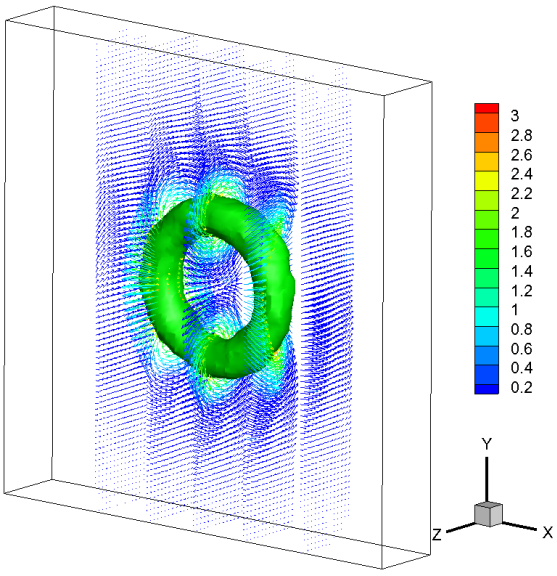


**Fig. 6** Iso-vorticity surface (0.13 voxels/voxel) from a simulation of vortex ring; Five planes of velocity vectors (color-coding indicates the magnitude of the velocity vector)

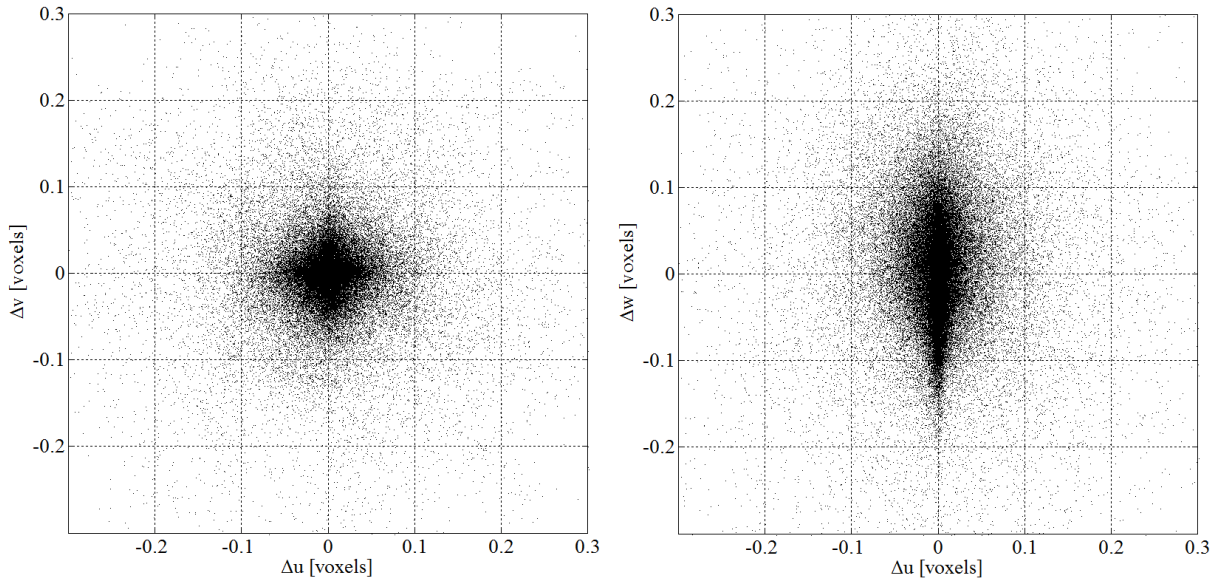


**Fig. 7** Scatter plots of the particle displacement error. *Left:* $x$ and $y$ displacement. *Right:* $x$ and $z$ displacement.

## 5. Conclusion

Dual-basis techniques including DBP, DB-MART and DB-SMART are discussed in current work. The new techniques introduce two important features of particle distribution into tomographic reconstruction, namely sparsity and spherical intensity distribution of particle. $l_1$-norm criterion is used as objective function to make a particle field sparse. A template of Gaussian intensity distribution combined with a correcting template proportional to identity is designed as an *a priori* knowledge to achieve a particle intensity with sub-voxel accuracy.

2D numerical tests show that DBP technique is superior to other approaches of particle reconstruction. It can completely recover the particle field with ppp < 0.15, and keep the quality factor $Q$ above 0.8 for ppp up to 0.30. Furthermore, DB-MART and DB-SMART both have better performance than traditional MART and SMART. The comparison of several different methods reveals the importance of the features of the sparsity of particle field and the particle intensity template.

Further study shows that DBP is sensitive to noise and difficult to be applied to 3D application due to its unaffordable memory usage and time consuming. Only DB-MART and DB-SMART are applicable for 3D application as a compromise. The parametric study on DB-SMART shows that it has good robustness regarding the standard deviation of template basis, random noise and background particles on images. A 3D application of synthetic vortex ring based on DB-SMART technique suggests that the new technique is able to handle a large-scale 3D reconstruction with high accuracy.

As a new concept for tomographic reconstruction, DBP needs more tests for understanding its performance on experimental data. There are many assessments are ongoing, such as the analysis of ghost particle, convergence and time cost.

Adrian, R. J. and J. Westerweel (2010). Particle image velocimetry, Cambridge University Press.

Atkinson, C. and J. Soria (2009). "An efficient simultaneous reconstruction technique for tomographic particle image velocimetry." Experiments in Fluids **47**(4-5): 553-568.

Barbu, I., C. Herzet, et al. (2011). Sparse models and pursuit algorithms for piv tomography. Forum on recent developments in Volume Reconstruction techniques applied to 3D fluid and solid mechanics.

Champagnat, F., P. Cornic, et al. (2013). "Tomographic PIV: particles vs blobs." PIV13 PDF PDF.

Chen, S. S., D. L. Donoho, et al. (1998). "Atomic decomposition by basis pursuit." SIAM journal on scientific computing **20**(1): 33-61.

Cornic, P., F. Champagnat, et al. (2013). "Computationally efficient sparse algorithms for tomographic PIV Reconstruction." Proceedings of PIV13.

Discetti, S., A. Natale, et al. (2013). "Spatial filtering improved tomographic PIV." Experiments in Fluids **54**(4).

Donoho, D. L. (2006). "Compressed sensing." Information Theory, IEEE Transactions on **52**(4): 1289-1306.

Elsinga, G. E., F. Scarano, et al. (2006). "Tomographic particle image velocimetry." Experiments in Fluids **41**(6): 933-947.

Gao, Q., H. Wang, et al. (2013). "Review on development of volumetric particle image velocimetry." Chinese Science Bulletin **58**(36): 4541-4556.

Gesemann, S., D. Schanz, et al. (2010). Recasting tomo-PIV reconstruction as constrained and L1-regularized non-linear least squares problem 15th Int. Symp. on Applications of Laser Techniques to Fluid Mechanics (Lisbon, Portugal).

Gordon, R., R. Bender, et al. (1970). "Algebraic reconstruction techniques (ART) for three-dimensional electron microscopy and X-ray photography." Journal of theoretical Biology **29**(3): 471-481.

Herman, G. T. and A. Lent (1976). "Iterative reconstruction algorithms." Computers in biology and medicine **6**(4): 273-294.

Lamarche, F. and C. Leroy (1990). "Evaluation of the volume of intersection of a sphere with a cylinder by elliptic integrals." Computer physics communications **59**(2): 359-369.

Mallat, S. G. and Z. Zhang (1993). "Matching pursuits with time-frequency dictionaries." Signal Processing, IEEE Transactions on **41**(12): 3397-3415.

Natterer, F. (1999). "Numerical methods in tomography." Acta Numerica **8**: 107-141.

Petra, S. and C. Schnörr (2010). TomoPIV Meets Compressed Sensing. AIP Conference Proceedings.

Petra, S., C. Schnörr, et al. (2007). "Tomographic image reconstruction in experimental fluid dynamics: Synopsis and problems." Mathematical Modelling of Environmental and Life Sciences Problems.

Petra, S., A. Schröder, et al. (2009). 3D tomography from few projections in experimental fluid dynamics. Imaging Measurement Methods for Flow Analysis, Springer**:** 63-72.

Scarano, F. (2013). "Tomographic PIV: principles and practice." Measurement Science and Technology **24**(1): 012001.

Scarano, F. and C. Poelma (2009). "Three-dimensional vorticity patterns of cylinder wakes." Experiments in Fluids **47**(1): 69-83.

Schanz, D., S. Gesemann, et al. (2013). "Non-uniform optical transfer functions in particle imaging: calibration and application to tomographic reconstruction." Measurement Science and Technology **24**(2): 024009.

Westerweel, J., G. E. Elsinga, et al. (2013). "Particle Image Velocimetry for Complex and Turbulent Flows." Annual Review of Fluid Mechanics **45**(1): 409-436.

Worth, N. A. and T. B. Nickels (2008). "Acceleration of Tomo-PIV by estimating the initial volume intensity distribution." Experiments in Fluids **45**(5): 847-856.